# Salient PM Rotor Topology Selection for a Zero-Speed Injection Based Sensorless Controlled Machine

*J Godbehere*, R Wrobel*, D Drury* and P H Mellor**

**Department of Electrical and Electronic Engineering, University of Bristol, Bristol, UK, jg7560@bristol.ac.uk*

**Keywords:** Sensorless control, machine design, high-frequency (HF) saliency, optimisation, finite element analysis (FEA).

## Abstract

In this paper a performance comparison of permanent magnet (PM) salient rotor topologies is conducted. The analysis has been carried out for a machine design case study where numerous design requirements need to be satisfied simultaneously. The requirements include: low speed, high torque, low-duty transient operation and zero-speed injection based sensorless control capability. The majority of work in this field treats the problem of PM machine design for sensorless control in a decoupled manner, where only the rotor or stator geometry is altered to achieve the required sensorless performance. Such an approach makes the performance comparison between various machine topologies challenging, as they are usually designed using different techniques, or initial design assumptions. In this paper a holistic design approach is used where the stator and rotor sub-assemblies are optimised together. This allows an unbiased comparison between the candidate machine designs. The following six salient rotor topologies have been considered: inset, spoke, flat-IPM, V-IPM, dual layer V-IPM and inset with cut-out. The most promising design variants have been selected and are discussed in detail, with the aim to select the best performing machine design for prototype manufacture.

## 1 Introduction

Sensorless control of machines aims to remove the requirement for a shaft mounted position sensor. The benefit of which is a reduction in system cost, improved reliability and a potential to reduce the overall system size and weight. A typical implementation of sensorless control across the full operational range combines a back EMF flux estimator for mid to high speed ranges and high frequency signal injection techniques for zero and low speed ranges [1], [2].

Machine design for sensorless control involves the requirements of the sensorless control algorithm to be embedded within the design process. The aim is to tailor the design to boost the electromagnetic characteristics that are critical to the success of the sensorless algorithm, whilst having minimal impact on the specified output performance requirements. The end product is a machine which will present a reliable rotor position signature across the full operating torque range, ensuring the sensorless control scheme will remain effective.

High frequency signal injection techniques require an electromagnetic signature to be incorporated into the machine design. A salient rotor, with a difference between the direct $(L_d)$ and quadrature $(L_q)$ inductances is the most common way of achieving this in a PM machine. The rotor positional signal becomes dependent on the saliency ratio $(L_q/L_d)$ being measurable across the full range of torque [3]. This can be challenging to achieve in a machine designed for high torque density and operating at a high flux density. This is because the measured values of inductance will change due to saturation and cause the magnitude of the saliency to decrease, in some cases even reverse [4].

Secondary magnetic effects introduce an error in the rotor position. This is mainly due to cross coupling between the direct (d) and quadrature (q) axis inductances. This error can be significant and cause a severe performance degradation [5]. Predicting and compensating for these secondary effects is time consuming as it varies with the rotor position and electric loading of the machine. Minimising this rotor position error is an important consideration in the design process [6].

The rotor topologies typically used for a sensorless control scheme are inset, spoke and IPM [1], [5]. This is because these topologies offer a high level of saliency, even when heavily saturated. It has been shown in literature that the choice of winding [7] and design of the stator [8] and rotor [9–12] have a significant impact on its sensorless control capability. However there is little published work on how to design a complete machine for sensorless control in a holistic manner.

The design optimisation methodology presented in [13] has been employed in this investigation. The proposed approach sizes the stator and rotor simultaneously within a single optimisation process. The benefit of this design process is that all the components which affect the sensorless control capability are accounted for. In addition all specification requirements are considered together, allowing machine designs to be generated which satisfy the target operating envelope and thermal behaviour, while being sensorless control capable. The aim of this paper is to use this optimisation technique to study a broad range of machine rotor topologies in a comprehensive manner. The most promising machine designs have been selected for more detailed analysis prior to the final selection.

## 2 Overview of the Machine Requirements

The operating envelope for the design case study is summarised in Table 1.

| Peak Power (kW) | Peak Torque (Nm) | Maximum Speed (RPM) | DC link voltage (V) |
|---|---|---|---|
| 1.5 | 47 | 420 | 28 |

Table 1 – Machine operating envelope specifications

The basic geometry of the machine has been derived from an initial design exercise [13]. Through a combination of analytical formulae and initial runs of the optimisation procedure a suitable pole and slot combination is chosen, as well as the stator bore, active length, number of turns and phase current. Target values for the back EMF constant and phase inductance are derived from this initial investigation and chosen so that the torque-speed envelope requirements are feasible within the constraints of the supply system [13].

Table 2 lists the geometrical data common for all machine-rotor variants analysed. Active materials used in the machine construction include aluminium conductors, N42UH PM and NO20 laminated steel.

| No. Poles (p) | No. Slots (q) | Stator Bore (D) (mm) | Active Length (L) (mm) | Air gap (g) (mm) | RMS phase current ($I_{prms}$) ($A_{rms}$) | Turns per slot ($N_s$) | Slot fill factor ($k_p$) |
|---|---|---|---|---|---|---|---|
| 16 | 72 | 112 | 35 | 1 | 64 | 4 | 0.465 |

Table 2 – Machine design choices for optimisation

## 3 Overview of the design methodology

The optimisation system comprises of a particle swarm optimisation routine and magneto-static, parametric, 2D finite element solver. A single operating point at full rated current is used to minimise computation time. This is the point at which the saliency will be at its lowest due to saturation in the iron.

A total of nine FE simulations are required to gather all the information required to assess a machine design [13]. Critical to this analysis is the prediction of the sensorless control performance. A differential inductance technique demonstrated in [14] is used within the optimisation to calculate components for the direct (1), quadrature (2) and two cross-coupling (3), (4) inductance components. A prediction of the sensorless performance can then be conducted as demonstrated in [14], [13] by introducing a high frequency current variation to these inductance components. Torque is calculated using flux linkage (5), as this is unaffected by slotting effects and is likely to be closer to the average torque over one electrical cycle.

$$L_d = \frac{\partial \lambda_d}{\partial i_d} \approx \frac{\lambda_{d(i_d - \Delta i_d, i_q)} - \lambda_{d(i_d, i_q)}}{\Delta I_d} \quad (1)$$

$$L_q = \frac{\partial \lambda_q}{\partial i_q} \approx \frac{\lambda_{q(i_d, i_q + \Delta i_q)} - \lambda_{q(i_d, i_q)}}{\Delta I_q} \quad (2)$$

$$L_{dq} = \frac{\partial \lambda_d}{\partial i_q} \approx \frac{\lambda_{d(i_d - \Delta i_d, i_q)} - \lambda_{d(i_d, i_q)}}{\Delta I_q} \quad (3)$$

$$L_{qd} = \frac{\partial \lambda_q}{\partial i_d} \approx \frac{\lambda_{q,(i_d, i_q + \Delta i_q)} - \lambda_{q,(i_d, i_q)}}{\Delta I_d} \quad (4)$$

$$T = \frac{3}{2} p \left( \lambda_{d(i_d, i_q)} I_q - \lambda_{q(i_d, i_q)} I_d \right) \quad (5)$$

Prior to the differential inductance calculation the optimum current angle *(γ)* is calculated from a series of six FE simulations and a curve fitting algorithm (6). The goal is to find the value of the current angle (γ) which gives maximum torque per amp (MTPA).

$$T = a_1 \sin\big(b_1(\gamma + c_1)\big) + a_2 \sin(b_2(\gamma + c_2)) \quad (6)$$

## 3 Fitness Function

A critical component of the design optimisation routine is the formulation of the fitness function. The fitness used within the optimisation is a single objective optimisation, but with multiple components which are summed together (7). The optimisation aims to maximise the value of fitness.

$$Fitness = \sum_{i=1}^{7} C_i F_i \quad (7)$$

Each fitness criteria *($F_i$)* has a possible maximum value of one and a minimum value of zero. In the optimisation algorithm $F_1$ is torque, $F_2$ saliency, $F_3$ the winding current density, $F_4$ the angular error of the sensorless algorithm, $F_5$ the d-axis inductance, $F_6$ the cross sectional area of the permanent magnets and $F_7$ the value of the split ratio (stator bore divided by the stator yoke outer diameter). The form of each fitness value is shown below (8), with the exception of the sensorless error which is defined in (9). The target values for the fitness function are shown in table 3, and the calibrated weightings ($C_i$) are shown in table 4. These have been found through trial and error and training of the optimisation process and are demonstrated to be effective in [13].

$$F_i = \frac{abs(X_{target} - X_{PSO})}{X_{target}} \quad (8)$$

$$F_4 = 1 - \frac{Error_{PSO}}{45} \quad (9)$$

| Torque (Nm) | Saliency | Current Density ($A/mm^2$) | Ld (µH) | PM area ($mm^2$) | Split Ratio |
|---|---|---|---|---|---|
| 47 | 2 | 27 | 373 | 65 | 0.76 |

Table 3 – Optimisation fitness function target values

| Torque ($C_1$) | Saliency ($C_2$) | Winding current ($C_3$) | Angular error ($C_4$) | D-axis inductance ($C_5$) | PM area ($C_6$) | Split Ratio ($C_7$) |
|---|---|---|---|---|---|---|
| 2.7 | 1.7 | 0.6 | 0.4 | 0.4 | 0.2 | 0.2 |

Table 4 – Optimisation fitness function coefficient weightings

## 4 Rotor Topology Selection

Six different rotor topologies have been selected for analysis: Inset, spoke, V-IPM, Flat-IPM, dual layer V-IPM and inset with "cut-outs". These six examples demonstrate some of the main categories of salient rotor types. The inset with "cut-out" topology has been selected based upon [15], which has been designed specifically for a sensorless control system.

The parameterisation of the stator is demonstrated in Figure 1, and the rotor variants in Figure 2. The same parameterisation of the stator is used throughout all optimisations.

The choice of number of particles in a swarm and weightings are based upon [16], [17], and have been shown to be effective when solving an electromagnetic optimisation problem. Each optimisation uses a swarm size of 30, runs for 120 iterations, and has been repeated 35 times. This provides a large sample size of data for analysis.

A fixed rotor position is used in the optimisation routine to minimise computation time. The performance at this rotor position will be maximised, however it is possible that values for the saliency and rotor position error could vary significantly at different rotor positions. A full electromagnetic analysis is therefore conducted afterwards to investigate this effect, and allow a more detailed comparison of the designs. The torque, saliency and rotor position error is calculated at several points over one electrical cycle. Within these tests the differential inductance technique discussed in section three is used to calculate the sensorless control capability. The torque is calculated using the Maxwell stress tensor, accounting for slotting effects. In addition an estimation for the torque-speed capability is carried out.

Each run of the optimisation produces a slightly different design. The best design for each of the six rotor types is selected for comparison based upon meeting the torque and speed requirement, the magnitude and variation of the saliency and the magnitude and variation of the rotor position error. The performance measures for the best machine designs are listed in Table 5 and layout of the machine geometries in Figure 3.

## 5 Analysis of Results

Table 5 includes the performance measures for the six rotor types. Each rotor type has met the main performance criteria: the torque and speed operating envelope, target conductor current density and a saliency above one for all operating points. The best design can therefore be selected based on the quality of the saliency profile, rotor position error and other secondary considerations.

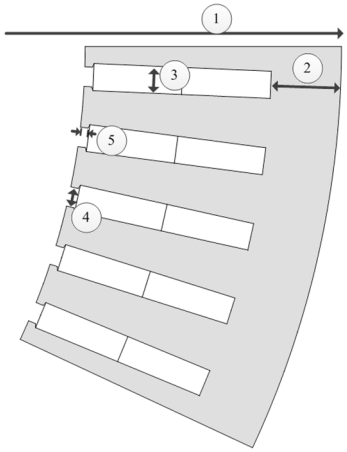


Figure 1 – Stator parameterisation

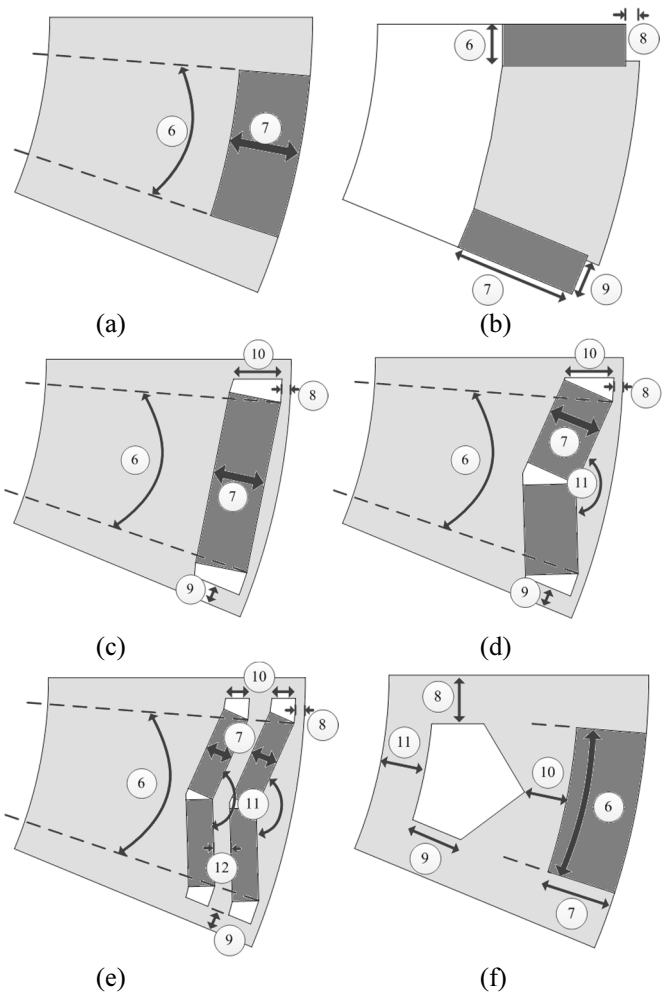


Figure 2 – Inset (a), Spoke (b), Flat-IPM (C), V-IPM (d), Dual layer V-IPM (e) and Inset with cut-out (f) rotor parameterisations

| Rotor Type | Fitness | Average Torque (Nm) | Average Saliency | Lowest Saliency | Average Position Error (°) | Peak Position Error (°) | Back EMF constant (Vs) (phase/rad) | Short circuit current (A) | Meet Torque/Speed? | Conductor current density ($A/mm^2$) | Magnetic Loading (T) | PM cross sectional area ($mm^2$) (per pole) | Weight (Kg) |
|---|---|---|---|---|---|---|---|---|---|---|---|---|---|
| Inset | 5.570 | 47.14 | 1.33 | 1.30 | -4.95 | -8.66 | 0.314 | 104.92 | Y | 27.09 | 0.83 | 65 | 8.91 |
| Spoke | 5.150 | 47.70 | 1.32 | 1.27 | -31.27 | -32.80 | 0.355 | 113.05 | Y | 27.32 | 0.94 | 63 | 8.95 |
| Flat IPM | 5.591 | 47.56 | 1.27 | 1.23 | -2.33 | -5.88 | 0.309 | 103.91 | Y | 27.00 | 0.82 | 71 | 9.27 |
| V IPM | 5.640 | 47.59 | 1.33 | 1.29 | -0.66 | -1.55 | 0.307 | 103.10 | Y | 27.05 | 0.81 | 69 | 9.20 |
| Dual V IPM | 5.483 | 47.64 | 1.33 | 1.29 | -0.97 | -3.32 | 0.305 | 104.73 | Y | 26.79 | 0.81 | 119 | 9.06 |
| Inset Cutout | 5.548 | 47.66 | 1.31 | 1.28 | -4.22 | -7.11 | 0.315 | 104.01 | Y | 27.10 | 0.83 | 65 | 9.15 |

Table 5 – Optimum machine designs performance comparison for each rotor type, at rated current

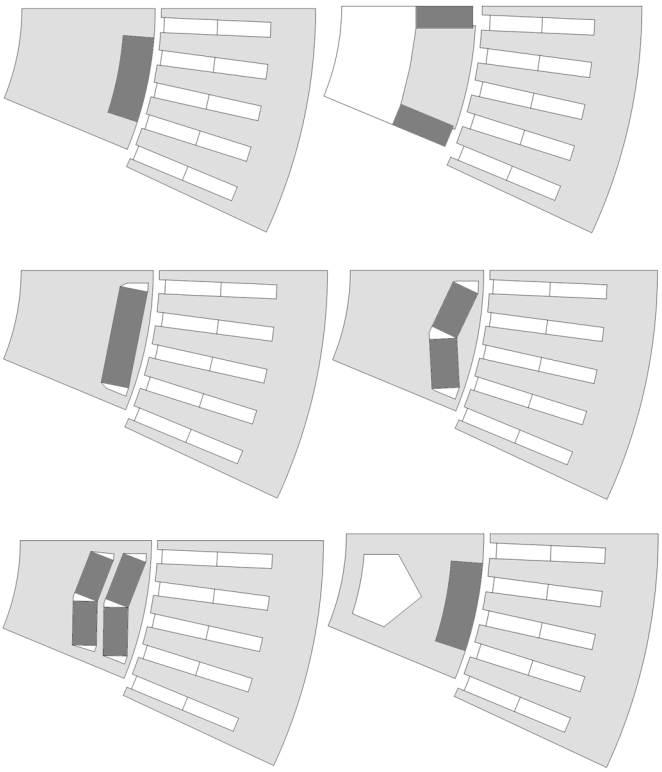

Figure 3 – Optimised machine geometries for each rotor type

The spoke topology has a characteristically high cross-coupling inductance leading to very high values for the rotor position error. If a sensorless control scheme were to be used with this rotor topology there would be a severe performance degradation on torque production. Because of this the spoke topology scores the lowest fitness value and is not considered for further discussion.

The inset with cut-out topology offers an increase in performance over the standard inset topology. A reduction in the rotor position error has been achieved whilst only affecting the magnitude of the saliency marginally.

The most promising rotor topology is the single layer V-IPM topology. It achieves saliency equal to the inset topology but adds a significant improvement to the rotor position error. The only downside is a slight increase in the PM material usage. The dual layer V-IPM on the other hand adds little to the performance in this case, achieving worse performance whilst using a significantly higher quantity of PM material.

Note that the stator design for each rotor type utilises an open slot topology. Further analysis has shown that this has a great impact on the performance of the machine and affects the magnitude of saliency, rotor position error and meeting the target operating envelope. Although the stator designs look similar, there are slight variations to the slot width, slot depth and back iron width between the different designs. These have been optimised to finely tune the performance for the individual rotor variants.

An estimate for total machine weight has been made for each rotor layout. In this estimate a simple round casing with a thickness of 15mm is used, and all other mechanical components are identical. The designs exhibit very similar values, the lightest being the Inset due to it having the highest split ratio.

The V-IPM topology and Inset with cut-out machine topologies show the best potential, and such have been selected for further analysis and comparison. Figure 4 shows the predicted torque versus speed performance for the two designs. Figure 5 shows the saliency and rotor error variation over one rotor electrical cycle at maximum current. It can be seen that the V-IPM topology experiences more saliency variation compared to the inset with cut-out variant, but the opposite for rotor position error.

Figure 6 demonstrates the torque calculated by a Maxwell stress tensor over one rotor electrical cycle, at rated current, for both machine topologies. The V-IPM topology has a peak to peak variation of 3.56 Nm, while the inset with cut-out has a variation of 5.74 Nm. Included is torque calculated using the predicted sensorless rotor position, assuming ideal machine drive operation. The V-IPM has a sensorless rotor position signal which follows the true position very closely. The inset with cut-out has a higher error, but it is small enough to have little effect on the average torque, or variation over one electrical cycle.

Finally figures 7 – 10 show the average saliency and rotor position error contour plots, including the maximum-torque-per-amp (MTPA) trajectory. These are the desirable points to drive the machine at from zero current, up to rated current. As expected the saliency starts off at a larger magnitude at low values of current, and decreases due to saturation in the machine iron. The rotor position error does not follow a similar

pattern, particularly for the V-IPM topology, as it peaks not at the rated current, but at around 60%. What is important however, is that the figures demonstrate that both topologies maintain a low rotor position error at all operating points.

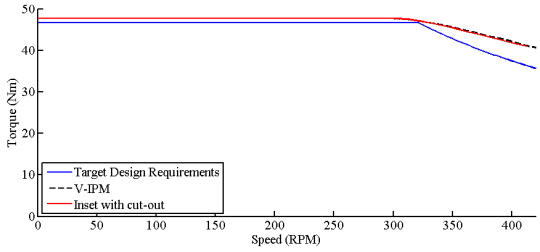


Figure 4 – Torque versus speed performance

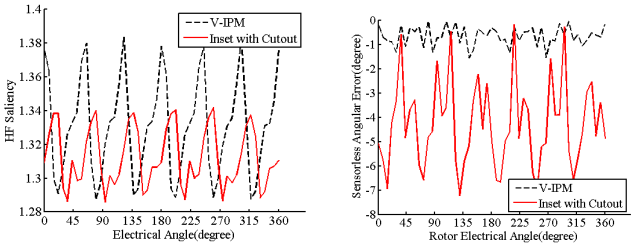


Figure 5 – High frequency saliency and sensorless rotor position error variation over one rotor electrical cycle at rated current

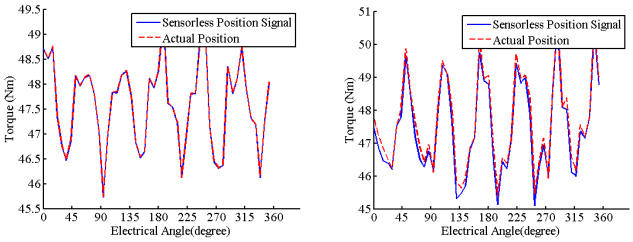


(a) (b)

Figure 6 – V-IPM (a) and inset with cut-out (b) torque variation, with actual rotor position and sensorless rotor position signal, over one rotor electrical cycle, at rated current

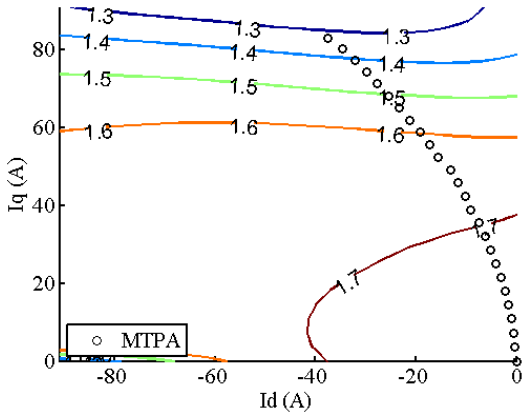


Figure 7 – V-IPM high frequency saliency variation, averaged over one rotor electrical cycle, including MTPA operating points

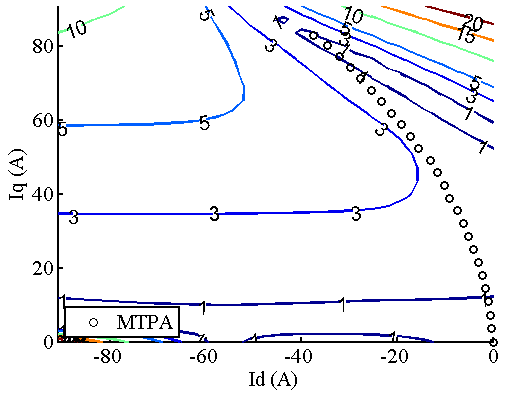


Figure 8 – V-IPM rotor position error magnitude variation, averaged over one rotor electrical cycle, including MTPA operating points

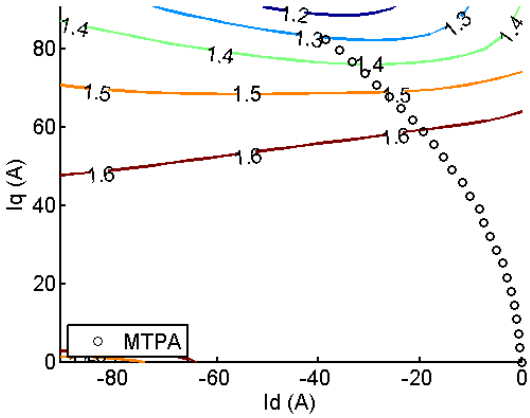


Figure 9 – Inset with cut-out high frequency saliency variation, averaged over one rotor electrical cycle, including MTPA operating points

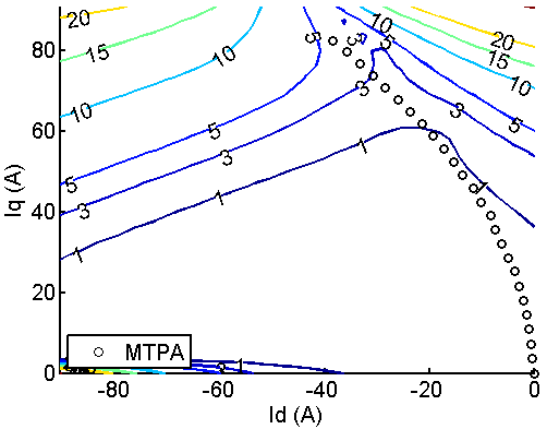


Figure 10 – Inset with cut-out rotor position error magnitude variation, averaged over one rotor electrical cycle, including MTPA operating points

## 6 Conclusion

Six different salient rotor topologies have been selected and parametrised for a design case study. Centre to the investigation is a design methodology utilising a full machine geometry optimisation. Each machine topology optimisation has been repeated multiple times to ensure a large sample data size. The best design of each rotor type has been selected and compared. An analysis of the sensorless performance variation with rotor position has been conducted for each of these designs at rated current.

Out of the six rotor topologies, only one machine design would be completely unsuitable for the specification. However the two best performing rotor topologies from the remaining designs are inset with cut-out and V-IPM. A detailed analysis of their sensorless performance, considering current loading and rotor position variation has been conducted. Both designs demonstrate excellent sensorless capability across all operating points whilst also meeting all other performance requirements.

The V-IPM topology has been selected for prototyping and hardware validation. This is based on the slight improvement in cogging torque and rotor position error. However an additional consideration is given to ease of manufacture, and the use of cheaper, parallel magnetised permanent magnets is preferred in this case.

## References


[1] R. Bojoi, M. Pastorelli, J. Bottomley, P. Giangrande, and C. Gerada, "Sensorless control of PM motor drives x2014; A technology status review," in *Electrical Machines Design Control and Diagnosis (WEMDCD), 2013 IEEE Workshop on*, 2013, pp. 168–182.

[2] S. Kim and S.-K. Sul, "Sensorless control of AC motor; Where are we now?," in *Electrical Machines and Systems (ICEMS), 2011 International Conference on*, 2011, pp. 1–6.

[3] N. Bianchi and S. Bolognani, "Influence of rotor geometry of an interior PM motor on sensorless control feasibility," in *Industry Applications Conference, 2005. Fourtieth IAS Annual Meeting. Conference Record of the 2005*, 2005, vol. 4, p. 2553 – 2560 Vol. 4.

[4] Y. Kano, T. Kosaka, N. Matsui, and M. Fujitsuna, "Sensorless-oriented design of concentrated-winding IPM motors for HEV drive application," in *Electrical Machines (ICEM), 2012 XXth International Conference on*, 2012, pp. 2709–2715.

[5] Y. Kano, "Sensorless-oriented design of IPMSM," in *Power Electronics Conference (IPEC-Hiroshima 2014 - ECCE-ASIA), 2014 International*, 2014, pp. 2457–2464.

[6] N. Bianchi, E. Fornasiero, and S. Bolognani, "Effect of Stator and Rotor Saturation on Sensorless Rotor Position Detection," *Industry Applications, IEEE Transactions on*, vol. 49, pp. 1333–1342, 2013.

[7] D. Reigosa, K. Akatsu, N. Limsuwan, Y. Shibukawa, and R. D. Lorenz, "Self-sensing comparison of fractional slot pitch winding vs. distributed winding for FW- and FI-IPMSMs based on carrier signal injection at very low speed," in *Energy Conversion Congress and Exposition, 2009. ECCE 2009. IEEE*, 2009, pp. 3806–3813.

[8] R. Wrobel, A. S. Budded, D. Holliday, P. H. Mellor, and P. Sangha, "Design Considerations for Permanent Magnet Brushless Machines for Zero-Speed Sensorless Position Estimation," in *Industry Applications Conference, 2006. 41st IAS Annual Meeting. Conference Record of the 2006 IEEE*, 2006, vol. 3, pp. 1494–1500.

[9] N. Bianchi and S. Bolognani, "Influence of Rotor Geometry of an IPM Motor on Sensorless Control Feasibility," *Industry Applications, IEEE Transactions on*, vol. 43, pp. 87–96, 2007.

[10] N. Bianchi, S. Bolognani, J.-H. Jang, and S.-K. Sul, "Comparison of PM Motor Structures and Sensorless Control Techniques for Zero-Speed Rotor Position Detection," *Power Electronics, IEEE Transactions on*, vol. 22, pp. 2466–2475, 2007.

[11] A. S. Budden, R. Wrobel, D. Holliday, P. H. Mellor, A. Dinu, P. Sangha, and M. Holme, "Impact of Rotor Design on Sensorless Position Estimation," in *IEEE Industrial Electronics, IECON 2006 - 32nd Annual Conference on*, 2006, pp. 787–792.

[12] R. Wrobel, A. S. Budden, D. Salt, D. Holliday, P. H. Mellor, A. Dinu, P. Sangha, and M. Holme, "Rotor Design for Sensorless Position Estimation in Permanent-Magnet Machines," *Industrial Electronics, IEEE Transactions on*, vol. 58, pp. 3815–3824, 2011.

[13] J. Godbehere, R. Wrobel, D. Drury, and P. H. Mellor, "Design methodology of a brushless IPM machine for a zero-speed injection based sensorless control," in *Energy Conversion Congress and Exposition (ECCE), 2015 IEEE*, 2015, pp. 5601–5608.

[14] N. Bianchi, D. Durello, and E. Fornasiero, "Multi-objective optimization of a PM Assisted Synchronous Reluctance Machine, including torque and sensorless detection capability," in *Power Electronics, Machines and Drives (PEMD 2012), 6th IET International Conference on*, 2012, pp. 1–6.

[15] N. Bianchi, S. Bolognani, A. Faggion, and E. Fornasiero, "Analysis and Experimental Tests of the Sensorless Capability of a Fractional-Slot Inset PM Motor," *Industry Applications, IEEE Transactions on*, vol. 51, pp. 224–231, Jan. 2015.

[16] J. Robinson and Y. Rahmat-Samii, "Particle swarm optimization in electromagnetics," *Antennas and Propagation, IEEE Transactions on*, vol. 52, pp. 397–407, Feb. 2004.

[17] R. Wrobel and P. H. Mellor, "Particle Swarm Optimisation for the Design of Brushless Permanent Magnet Machines," in *Industry Applications Conference, 2006. 41st IAS Annual Meeting. Conference Record of the 2006 IEEE*, 2006, vol. 4, pp. 1891–1897.